ELSEVIER

Journal of Neuroscience Methods 148 (2005) 94–102

JOURNAL OF NEUROSCIENCE METHODS

www.elsevier.com/locate/jneumeth

Near infrared two-photon excitation cross-sections of voltage-sensitive dyes

Jonathan A.N. Fisher [a,*], Brian M. Salzberg [b,c], Arjun G. Yodh [a]

[a] *Department of Physics and Astronomy, University of Pennsylvania, 209 South 33rd Street, Philadelphia, PA 19104, USA*
[b] *Department of Neuroscience, University of Pennsylvania School of Medicine, Philadelphia, PA 19104, USA*
[c] *Department of Physiology, University of Pennsylvania School of Medicine, Philadelphia, PA 19104, USA*

Received 4 April 2005; received in revised form 15 June 2005; accepted 28 June 2005

Abstract

Microscopy based on voltage-sensitive dyes has proven effective for revealing spatio-temporal patterns of neuronal activity in vivo and in vitro. Two-photon microscopy using voltage-sensitive dyes offers the possibility of wide-field visualization of membrane potential on sub-cellular length scales, hundreds of microns below the tissue surface. Very little information is available, however, about the utility of voltage-sensitive dyes for two-photon imaging purposes. Here we report on measurements of two-photon fluorescence excitation cross-sections for nine voltage-sensitive dyes in a solvent, octanol, intended to simulate the membrane environment. Ultrashort light pulses from a Ti:sapphire laser were used for excitation from 790 to 960 nm, and fluorescein dye was used as a calibration standard. Overall, dyes RH795, RH421, RH414, di-8-ANEPPS, and di-8-ANEPPDHQ had the largest two-photon excitation cross-sections ($\sim 15 \times 10^{-50}$ cm^4 s photon^{-1}) in this wavelength region and are therefore potentially useful for two-photon microscopy. Interestingly, di-8-ANEPPDHQ, a chimera constructed from the potentiometric dyes RH795 and di-8-ANEPPS, exhibited larger cross-sections than either of its constituents.

Keywords: Voltage-sensitive dyes; Potentiometric dyes; Two-photon microscopy; Cross-sections; Styryl dyes; Nonlinear optical properties; Chimeric dyes

1. Introduction

Functional imaging of neuronal activity in three dimensions offers new possibilities for understanding brain physiology. Since the functional architecture of the brain is three-dimensional, one goal of neuroimaging is to accurately resolve neuronal activity in three-dimensions with high spatial- and temporal-resolution. The work of Llinas and others, for example, has shown that large-scale aspects of brain function can originate from electrical properties of individual neurons (Llinas, 1988; Llinas et al., 1998), underscoring the need for cellular and sub-cellular scale imaging. Measurements of membrane potential in small neurons and their processes, however, are extremely difficult using traditional electrode techniques. Measurements of macroscopic tissue volumes are similarly difficult, requiring large impractical electrode arrays.

The use of voltage-sensitive (potentiometric) dyes as molecular voltmeters (Cohen and Salzberg, 1978; Salzberg, 1983) is currently the only optical technique enabling direct measurements of neuronal membrane potential. The sensitivity of this methodology ranges from ∼10 mV scales, relevant for subthreshold membrane potential dynamics, to the ∼100 mV scales associated with action potentials. Voltage-sensitive dyes have proven to be effective for measuring electrical activity in neurons in vitro (Contreras and Llinas, 2001; Grinvald et al., 1983; Salzberg et al., 1973, 1977; Yuste et al., 1997) and in vivo (Grinvald et al., 1994; Orbach and Cohen, 1983; Petersen et al., 2003). To date, several studies have visualized voltage-sensitive dye responses in three-dimensions using one-photon fluorescence in vivo (Kleinfeld and Delaney, 1996; Petersen et al., 2003), and recently gradient-index (GRIN) lens optics and computational optical sectioning techniques have been used to achieve

* Corresponding author. Tel.: +1 215 573 3463; fax: +1 215 573 6391.
E-mail address: aafisher@physics.upenn.edu (J.A.N. Fisher).

0165-0270/$ – see front matter © 2005 Elsevier B.V. All rights reserved.
doi:10.1016/j.jneumeth.2005.06.027

high-speed three-dimensional microscopy with voltage-sensitive dyes in near surface tissues (Fisher et al., 2004). However, in all these studies optical sectioning is inherently limited by one-photon fluorescence microscopy techniques; i.e. the images are sensitive to fluorescence from the entire depth of focus and do not explicitly reject out-of-focus light.

Two-photon laser scanning microscopy (Denk et al., 1990) enables true three-dimensional imaging because of its intrinsic optical sectioning properties. Additionally, high contrast images can be obtained from deeper within biological tissues compared to confocal microscopy (Centonze and White, 1998). Since its inception, two-photon laser scanning microscopy has found wide-spread applicability throughout the field of neuroscience, both in vitro (Mainen et al., 1999; Yuste et al., 1997) and in vivo (Helmchen et al., 2001; Stosiek et al., 2003; Svoboda et al., 1999; Yoder and Kleinfeld, 2002). Calcium Green, GFP, and other fluorophores with absorption peaks in the blue are among the most widely used dyes for in vivo studies, in part because their peak absorption wavelength can be reached by two photons within the tuning range of most commercially available pulsed laser sources. Calcium-indicators yield large signals following two-photon excitation and can reveal rapid intracellular Ca^{2+} concentration changes dependent upon action potentials (Svoboda et al., 1997), but they most certainly do not provide a direct measurement of electrical activity.

Second harmonic generation (SHG) imaging (Hellwarth and Christensen, 1974; Sheppard et al., 1977) also provides inherent optical sectioning, and has recently been used in conjunction with voltage-sensitive dyes (Campagnola et al., 1999; Dombeck et al., 2004; Millard et al., 2003) to produce exceptional images of activity in cultured neurons. However, because SHG is a parametric nonlinear process, the resulting second harmonic wave travels predominantly in the same direction as the incident light (Mertz and Moreaux, 2001) and yields signal in the reflectance direction only after backscattering. By contrast, even at the scale of a single fluorophore, fluorescence emission following two-photon absorption of polarized light by membrane-bound voltage-sensitive dyes leads to a symmetric dipole radiation distribution (Lakowicz, 1999). In sub-surface tissue imaging conditions, where the excitation volume is small compared to the imaging depth, photons are generally assumed to be emitted isotropically (Oheim et al., 2001). These factors make two-photon microscopy preferable to SHG for backward detection, a critical criterion for in vivo imaging.

Albota, Xu and Webb have measured two-photon excitation cross-sections for a variety of biologically relevant molecular fluorophores (Albota et al., 1998; Xu, 2000; Xu and Webb, 1996). Very little information, however, exists on the suitability of voltage-sensitive dyes for two-photon imaging purposes (Hess and Webb, 1998). To this end, we have analyzed the two-photon spectral properties of some of the most common voltage-sensitive dyes, including recent novel dyes di-8-ANEPPDHQ (Obaid et al., 2004) and RH1692 (Shoham et al., 1999). We also included in our study Nile Blue A, which is a lipophilic membrane-permeant potentiometric dye (Beeler et al., 1981; Cohen et al., 1974; Vergara et al., 1978). Using a ratiometric method (Albota et al., 1998) with fluorescein as a reference, two-photon excitation cross-sections were obtained for nine voltage-sensitive dyes at incident wavelengths ranging from 790 to 960 nm. We used octanol as a solvent to approximate the environment of these dyes when bound to membrane (Sims et al., 1974) and we identified dyes with comparatively high cross-sections in this spectral region. Our investigation of the novel napthylstyryl-pyridinium "chimera" dye di-8-ANEPPDHQ, which is a combination of an RH795 (Grinvald et al., 1994) quarternary ammonium head group and a di-8-ANEPPS (Bedlack et al., 1992) chromophore, revealed that its two-photon excitation cross-section in this spectral region was larger than that of either of its constituent components.

2. Materials and methods

2.1. Background theory

In two-photon absorption, an atom or molecule simultaneously absorbs two photons and makes a transition from its ground state to an excited state. Assuming no linear (i.e. one-photon) absorption, the two-photon absorption of light propagating through an optically thin sample of C molecules per unit volume (cm^{-3}) is characterized by the following differential equation for the input light intensity I:

$$\frac{dI}{dz} = -\beta I^2. \tag{1}$$

Here I is the source intensity ($erg\,cm^{-2}\,s^{-1}$), and β is the two-photon absorption coefficient. The two-photon absorption coefficient, β, can also be expressed in terms of the two-photon cross-section, Σ, i.e.

$$\beta = 2C\frac{\Sigma}{\hbar\omega}, \tag{2}$$

where ω is the angular frequency of the incident light field; the factor of 2 arises because two photons are absorbed, and Σ has cgs units of $cm^4\,s$. In Eq. (2), $\hbar\omega$ is the energy per photon ($erg\,photon^{-1}$) at the excitation wavelength. The informal unit for Σ is the Goeppert-Mayer (GM), where $1\,GM = 10^{-50}\,cm^4\,s\,photon^{-1}$. Σ is described as a "cross-section" in order to establish a two-photon analog to the linear (one-photon) absorption cross-section, which has true units of area. The extra factor of cm^2 is due to the extra factor of I in Eq. (1).

The two-photon absorption cross-section, in turn, can be defined in terms of the material third-order susceptibility, $\chi^{(3)}$, i.e.

$$\Sigma = \frac{4\pi^2\hbar\omega^2\,\mathrm{Im}\,\chi^{(3)}}{C\eta^2c^2}. \tag{3}$$

Here η is the real part of the linear index of refraction at ω, and c is the speed of light.

$\chi^{(3)}$ is a fourth-rank tensor. Thus the most general description of the third-order nonlinear susceptibility $\chi^{(3)}_{ijkl}(\omega_4 = \omega_1 + \omega_2 + \omega_3)$ contains 81 terms. Significant simplifications, however, arise when the medium is an isotropic collection of random molecules, and when nonlinear terms such as $\chi_{ijkl}(\omega = \omega + \omega - \omega)$ are large compared to the other terms, e.g. as a result of small resonant denominators. In this case, $\chi^{(3)}$ Eq. (3) is well described as a frequency-dependent scalar (Hanna et al., 1979).

The two-photon absorption cross-section, Σ, can be measured by absorption and excitation spectroscopy techniques (Birge, 1983). Absorption spectroscopy measures the attenuation of the incident light as it passes through a sample of known concentration and thickness. Excitation spectroscopy measures the light emitted by the molecules following absorption. Generally, absorption measurements are difficult because the high incident intensities required to generate measurable absorption signals also lead to saturation, excited-state absorption, and photobleaching (Albota et al., 1998). On the other hand, for molecules with reasonably large quantum efficiencies, q ($>10^{-3}$), the fluorescence signal is readily detectable and can yield accurate measurements of Σ if q is known. Here q is the number of emitted photons by the molecule per absorbed photon. The two-photon excitation cross-section, σ_2 is the product of Σ and the two-photon quantum efficiency, q_2, defined as the number of emitted photons by the molecule per *pair* of absorbed photons:

$$\sigma_2 = q_2 \Sigma. \tag{4}$$

In two-photon microscopy the measured signal is typically fluorescence emission, and therefore σ_2 is generally a more useful figure of merit than Σ.

Xu and Webb (1996) have shown that for mode-locked laser sources, the time-averaged fluorescence signal $\langle F(t)\rangle$ (photons s^{-1}) detected by a spectroscopic system with collection efficiency φ and time-averaged illumination power $\langle P(t)\rangle$ (photons s^{-1}) is

$$\langle F(t)\rangle \approx \frac{1}{2}\varphi q_2 \Sigma C \frac{g_p}{f\tau}\frac{8\eta\langle P(t)\rangle^2}{\pi\lambda}. \tag{5}$$

Here C is the concentration of fluorophores in the sample (cm^{-3}), f is the repetition rate of the pulsed laser, τ is the laser pulse width, g_p is a numerical constant of order unity, λ is the center wavelength of the laser pulse, and η is the real part of the linear index of refraction at ω. The quantity $\frac{g_p}{f\tau}\frac{8\eta\langle P(t)\rangle^2}{\pi\lambda}$ accounts for the temporal shape of the pulses and the spatial profile of the beam in the excitation volume (Hopt and Neher, 2001; Xu and Webb, 1996); to compute this quantity the sample thickness is assumed much larger than the depth of focus of the imaging system, and diffraction limited high numerical aperture focusing (Richards and Wolf, 1959; Sheppards and Matthews, 1987) is also assumed.

Since the rate of two-photon absorption (TPA) depends on the spatial and temporal excitation beam profiles, Albota et al. (1998) introduced a ratiometric technique whereby σ_2 of an unknown sample is deduced from identical measurements made of a reference sample with known values of σ_2. Within this approach the two-photon excitation cross-section, σ_{2S}, of an unknown sample is

$$\sigma_{2S}(\lambda) = q_{2S}\Sigma_S(\lambda) = q_{2R}\Sigma_R(\lambda)\frac{\varphi_R C_R}{\varphi_S C_S}\frac{\langle P_R(t)\rangle^2}{\langle P_S(t)\rangle^2}\frac{\langle F(t)\rangle_S}{\langle F(t)\rangle_R}\frac{\eta_R}{\eta_S}, \tag{6}$$

where subscripts S and R indicate "sample" and "reference," respectively, and the cross-sections are written explicitly as a function of wavelength to remind us about their wavelength-dependence. In our measurements we monitored the second harmonic signal SHG(t) from a small fraction of the incident beam that was diverted through a beta-barium borate (β-BaB_2O_4, or "BBO") SHG crystal (Inrad, Northvale, NJ, USA); the time-averaged second harmonic, $\langle$SHG(t)$\rangle$, is directly proportional to $\langle P(t)\rangle^2$.

2.2. Experimental setup

The optical setup for cross-section measurements is shown in Fig. 1. In the experiment, C_R and C_S are known, Σ_R, η_R, and η_S are taken from the literature, and $\langle F(t)\rangle$, φ_R, φ_S, and $\langle P(t)\rangle^2$ are measured for each sample. The laser excitation source was a mode-locked Ti:sapphire laser (Mira Basic, Coherent Inc., Santa Clara, CA, USA) with a 76 MHz repetition rate. The laser was pumped by an 8 W multi-line argon-ion laser (Innova 310, Coherent Inc., Santa Clara, CA, USA). While two different optics sets were used to span the spectral region from 790 to 960 nm, optics sets that span the range of 720–980 nm are now available. The wavelength was confirmed with an external spectrum analyzer (Ocean Optics Inc., Dunedin, FL, USA). As noted above, a small fraction of the excitation beam was focused onto a BBO SHG crystal (Inrad, Northvale, NJ, USA) to record a signal proportional to $\langle P(t)\rangle^2$, which was time-averaged over the measurement period. The ratio of reference and sample values of $\langle$SHG(t)$\rangle$ was within the range of 1 ± 0.01. To minimize distortion of the beam profile, a $\lambda/2$ plate and Glan–Thompson polarizer were used to adjust the average excitation power at the sample to be ~10 mW.

Pulse widths were measured with a home-built background-free autocorrelator (Angerer, 1998; Angerer et al., 1999). The pulse-width measured just before the sample was ~200 fs. The beam was expanded with a 5× Gallilean beam-expander in order to back-fill an N.A. 0.4 objective (Carl Zeiss AG, Gottingen, Germany); the approximate spot size in the sample was ~3 μm. TPA-induced fluorescence was collected at 90° re-focused onto the slit of a monochromator (Thermo Jarrell-Ash Corporation, Franklin, MA, USA). The fluorescence signal was detected by a photomultiplier tube (Hamamatsu R943-02, Hamamatsu Photon-

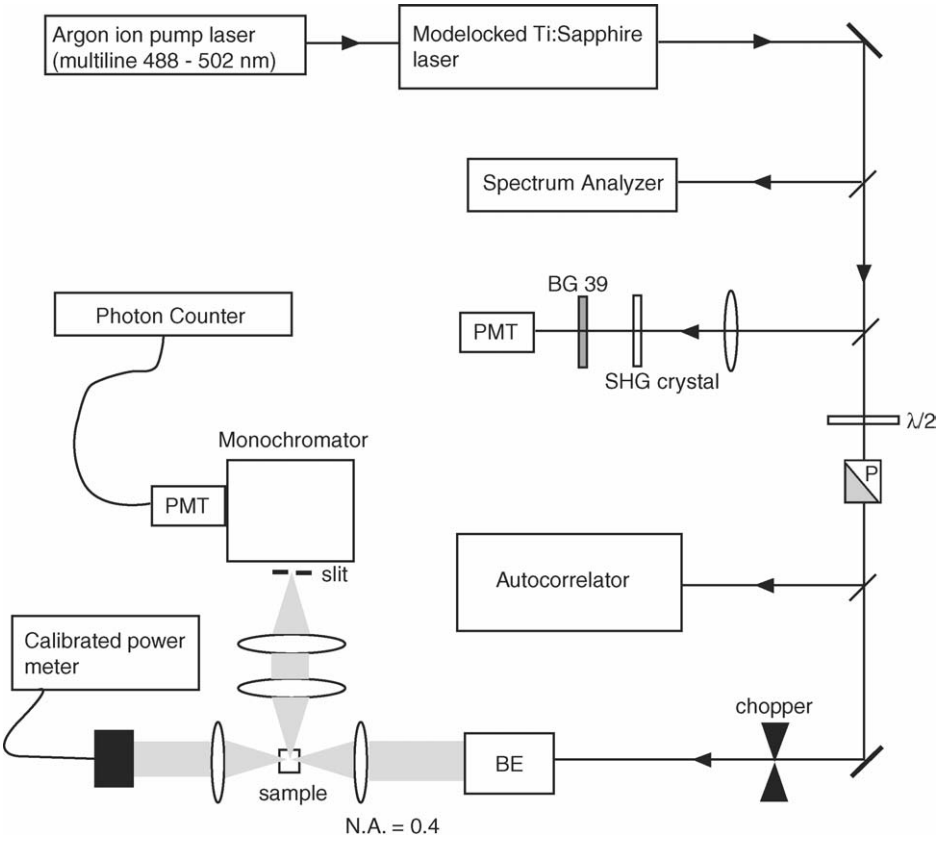

Fig. 1. Cross-section measurement setup. BG 39: Schott glass absorption filter, PMT: photomultiplier tube, SHG: second harmonic generating BBO crystal (Inrad), λ/2 = half wave plate, P: Glan–Thompson polarizer, BE: beam expander (5×).

ics, Hamamatsu City, Japan) which then fed a gated photon counter (SR400, Stanford Research Systems, Sunnyvale, CA, USA). The excitation beam passed through a chopper which provided a reference signal enabling the photon counter to perform background subtracted integration. Average power levels of the incident light were also monitored by refocusing the excitation beam onto a calibrated power meter (Newport Corporation, Irvine, CA, USA).

One centimeter thick sample cells were used to ensure that the entire focal volume of the excitation light was contained within the sample. We accounted for small absorptive losses by measuring the location of the focal volume within the cuvette and using linear absorption theory with the known molar extinction coefficients ε of the fluorophores. For all measurements the linear absorption was negligible (i.e. its effects were much smaller than the systematic uncertainty in the measurements).

2.3. Calculation of collection efficiency

Because the monochromator grating efficiency is wavelength-dependent, it was necessary to measure φ for each wavelength setting used. φ depends on the product of several factors: photomultiplier tube quantum efficiency, solid angle of collection (expressed as a percentage of 4π radians), monochromator transmission, quartz cuvette transmission, and the fluorophore emission spectrum. Monochromator transmission was measured using a white light source emitting into the 90° fluorescence collection path to mimic fluorescence emission. To this end, white light was focused at the point of two-photon excitation in the sample cuvette, and care was taken to ensure that all subsequently diverging light was contained within the fluorescence collection solid angle (a function of fluorescence collection optics and the acceptance numerical aperture of the monochromator). First, the reference intensity was measured without the monochromator in the optical path; then the monochromator was placed in the position used throughout the entire experiment. A spectrophotometer (Ocean Optics, Dunedin, FL, USA) replacing the fluorescence-collection PMT was used to generate transmission curves as the monochromator scanned over all relevant wavelength settings. The uncertainty in calculation of φ was by far the largest source of systematic error. This error reflects uncertainty in monochromator transmission as a function of wavelength, and errors due to numerical integration of the transmission spectrum, since the fluorescein reference and experimental sample were typically measured at different monochromator settings. By repeating the monochromator transmission measurement procedure using a focused white light source, we obtained a standard deviation for this aspect of the measurement. Error introduced by the numerical integration of the dye emission spectrum was estimated by

Table 1
Sample summary

Fluorophore	Source	$\lambda_{abs/em}$ (nm)	Concentration (μM)	Reference
di-8-ANEPPS	L. Loew	433/625	90	Bedlack et al. (1992)
di-8-ANEPPDHQ	L. Loew	500/620	16	Obaid et al. (2004)
RH795	Molecular Probes	530/640	95	Grinvald et al. (1994)
RH414	Molecular Probes	525/636	150	Grinvald et al. (1988)
RH237	Molecular Probes	550/676	142	Gogan et al. (1995)
RH421	Molecular Probes	532/648	97	Grinvald et al. (1983)
RH1692	R. Hildesheim	600/680	117	Shoham et al. (1999)
Merocyanine 540	Eastman Kodak[a]	533/615	128	Davila et al. (1973)
Nile Blue A	Chroma Gesellschaft[b]	649/660	118	Vergara et al. (1978)

Absorption and emission wavelengths are experimentally measured values in octanol.
[a] Eastman Kodak, Rochester, New York.
[b] Chroma Gesellschaft-Schmid & Co., Stuttgart, Germany.

comparing the results of numerical integration while varying (1) numerical method, (2) interpolation resolution, and (3) integration limits. We estimated the systematic error in measurements of two-photon cross-sections to be ±30%, comparable to the uncertainty reported by Albota et al. (1998). This number represents the standard deviation obtained as a result of propagating estimated errors in both sample and reference fluorescence collection efficiencies, φ_S and φ_R. Other significant sources of systematic error were constant for both sample and reference, and thus cancelled out.

2.4. Sample preparation

Sample preparation and the sample sources are listed in Table 1. Selected chemical structures are shown in Fig. 2. Large stock solutions were prepared and then diluted to concentrations of ∼100 μM. The reference sample was fluorescein in H_2O at pH 13. Two-photon cross-sections are known for this reference sample (Albota et al., 1998; Xu, 2000). For all other samples, octanol was used as a solvent. For solubility reasons, some samples were first prepared at high concentration in other solvents before adding octanol. For example, RH1692 was first dissolved in a small quantity of ethanol; di-8-ANEPPS and di-8-ANEPPDHQ were first prepared in a highly concentrated stock solution of DMSO/Pluronic. In these cases, solvents other than octanol comprise less than 1% of the total solution volume.

2.5. Measurement procedure

For each wavelength, the fluorescein reference sample was first measured, and then the rest of the samples were measured. Each measurement was followed by a blank sample in order to measure background stray light. Then the fluo-

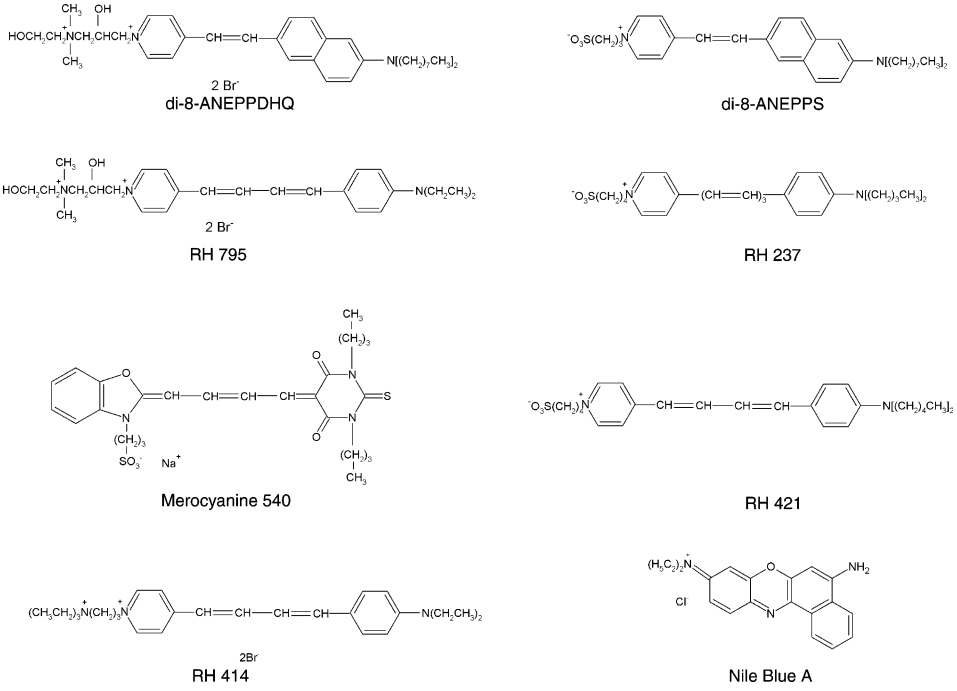

Fig. 2. Chemical structures of voltage-sensitive dyes used in this investigation.

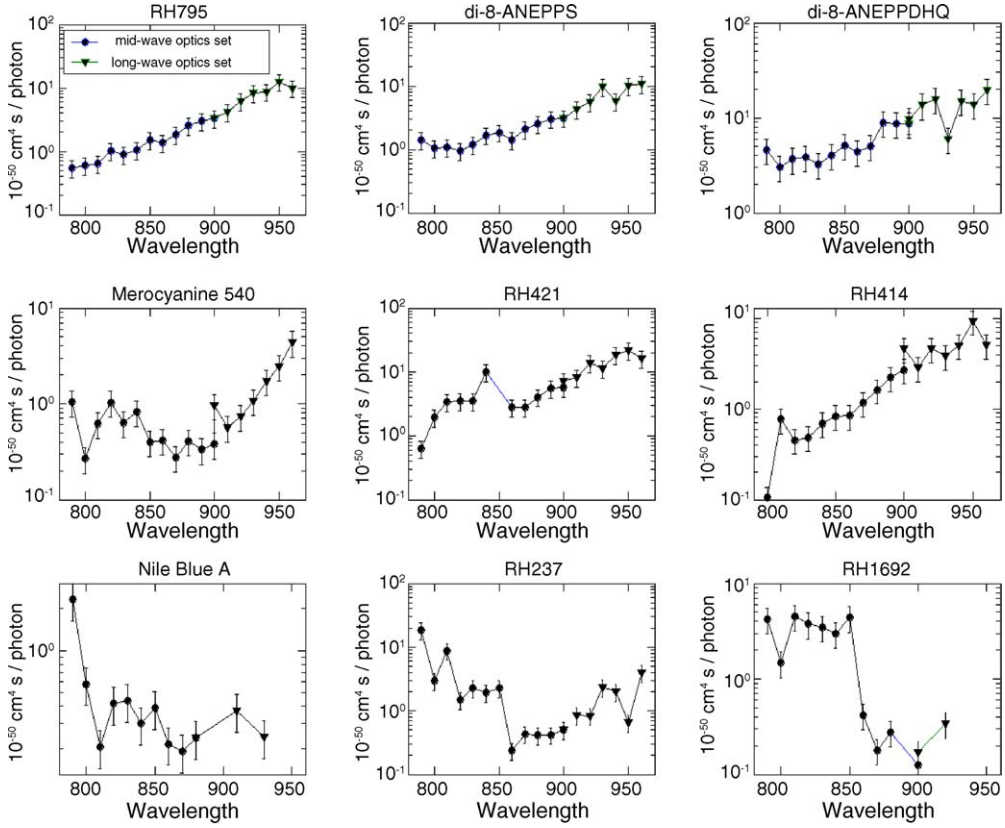

Fig. 3. Log-scale plots of two-photon excitation (TPE) cross-sections of voltage-sensitive dyes. Values of σ_2 are plotted in units of 10^{-50} cm^4 s photon^{-1} as a function of wavelength (nm): (●) mid-wavelength optics set (790–900 nm), (▼) long-wavelength optics set (900–960 nm). Systematic error for σ_2 is ±30% for each point.

rescein reference was measured again. The monochromator was tuned to the peak of the emission spectrum for each fluorophore. Before placing the sample in the cuvette holder, the average excitation power was measured with the calibrated power meter. For each sample at each wavelength, integrated fluorescence photon counts from the SR400 and the averaged SHG signal were recorded. Background counts were subtracted from the total integrated fluorescence photon counts. Integration times were 20–40 s. Intensity tests confirming the power-squared dependence of the fluorescence were performed by measuring the integrated fluorescence at various excitation intensities. Excitation intensities were measured with the calibrated power meter. The results were plotted on a log–log scale and fit to a line, the slope of which yielded the power-dependence exponent.

3. Results

3.1. Two photon excitation cross-sections

TPE cross-section measurements, σ_2, for all samples are shown in Fig. 3. Cross-section values are in units of the Goeppert-Mayer (GM), where 1 GM = 10^{-50} cm^4 s photon^{-1}. Values at selected wavelengths are listed in Table 2.

Table 2
Values of σ_2 at selected wavelengths

Dye	800 nm	840 nm	880 nm	920 nm	960 nm
di-8-ANEPPS	1.4 ± 0.4	1.7 ± 0.5	2.5 ± 0.8	5.6 ± 1.7	10 ± 3.0
di-8-ANEPPDHQ	3.0 ± 0.9	4.0 ± 1.2	8.8 ± 2.6	16 ± 4.8	19 ± 5.9
RH795	0.6 ± 0.2	1.0 ± 0.3	2.5 ± 0.8	6.3 ± 1.9	10 ± 3.0
RH414	0.10 ± 0.03	0.69 ± 0.21	1.6 ± 0.5	4.6 ± 1.4	12 ± 3.6
RH421	1.9 ± 0.5	10 ± 3.0	4.0 ± 1.2	13.6 ± 4.1	16 ± 4.8
RH237	8.9 ± 2.6	2.3 ± 0.7	0.42 ± 0.1	0.84 ± 0.2	3.9 ± 1.2
RH1692	1.5 ± 0.4	–	0.27 ± 0.08	0.68 ± 0.2	–
Nile Blue A	0.6 ± 0.2	0.13 ± 0.04	0.24 ± 0.07	–	–
Merocyanine 540	0.27 ± 0.08	0.83 ± 0.25	0.41 ± 0.1	0.74 ± 0.2	4.4 ± 1.3

Cross-sections are given in GM (1 GM = 10^{-50} cm^4 s photon^{-1}), and dashes represent measurements with insufficient signal-to-noise.

Table 3
Linearity tests for power-squared fluorescence dependence

Dye	Slope
RH795	2.05 ± 0.06
RH421	1.96 ± 0.06
di-8-ANEPPS	2.06 ± 0.08
di-8-ANEPPDHQ	1.95 ± 0.08

Values are slope of logarithmic plot of fluorescence (AU) as a function of peak excitation intensity at 920 nm.

All of the blue-green-absorbing dyes (RH795, RH414, RH421, RH237, di-8 dyes, and Merocyanine 540) exhibit increases in cross-section between 900 and 960 nm. This is almost certainly because the excitation photon wavelength approaches twice the peak one-photon absorption wavelength of the blue-green-absorbing dyes. In fact, all of the blue-green-absorbing dyes except for RH237 exhibited increases of over an order of magnitude as λ_{ex} varied from 790 to 960 nm. Both Nile Blue A and RH1692, the two red-absorbing dyes in the study, exhibit an overall decrease in cross-section between 790 and 960 nm. The high values near 790 nm are most likely due to one-photon absorption in the red absorption tail, which extends to 750 nm in both dyes. Very little spectral discontinuity was observed when changing optics sets.

3.2. Linearity tests

Table 3 reports the results of linearity tests for several fluorophores. The deviation from a pure intensity-squared law is within ±6% for all samples. These results confirm that the measured fluorescence emission was indeed true two-photon induced fluorescence.

4. Discussion

4.1. Comparison with one-photon absorption spectra

When plotted as a function of $\lambda_{ex}/2$, all of the TPE cross-section spectra mimic the trends of their one-photon absorption spectra. di-8-ANEPPS was the only fluorophore for which the two-photon absorption peak was within our tuning range. A small peak in TPE cross-section at 850 nm is observed in this case, which is likely a blueshifted correlate of twice the one-photon absorption peak expected at 866 nm. Other non-resonance features in Fig. 3 are also likely to be physical trends corresponding to one-photon absorption spectra. For instance, the small peak at 425 nm in the one-photon absorption spectrum of Nile Blue A is found in the TPE spectrum as a blueshifted peak at 830 nm (Fig. 4).

4.2. di-8-ANEPPDHQ versus RH795 and di-8-ANEPPS

A striking result in this study is the greatly increased cross-section of the chimeric molecule di-8-ANEPPDHQ compared with that of its constituent components (Fig. 5). No peak in the TPE spectrum in this range is observed, and none is expected since the one-photon absorption maximum is at 500 nm. However, the chimera TPE cross-section values were double those of RH795 and di-8-ANEPPS over the entire tuning range. Di-8-ANEPPS has recently been shown to offer advantages for imaging of mammalian neuronal networks (Obaid et al., 2004). Combined with the fact that 790–960 nm is a typical tuning range for most of the commercially available laser sources for two-photon microscopy, di-8-ANEPPDHQ shows significant promise for two-photon voltage-sensitive dye imaging.

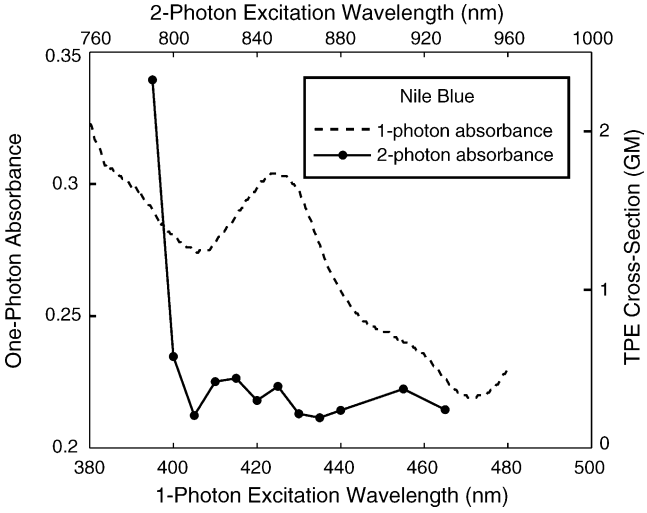

Fig. 4. Comparison of linear (one-photon) absorbance and two-photon excitation (TPE) cross-sections (σ_2) for Nile Blue A. Absorbance (defined as $-\log_{10}(I/I_0)$, where I/I_0 is the sample transmittance) and σ_2 (in units of 10^{-50} cm^4 s photon^{-1}) are plotted as a function of excitation wavelength (nm) (bottom and top axes correspond to one- and two-photon excitation wavelengths, respectively).

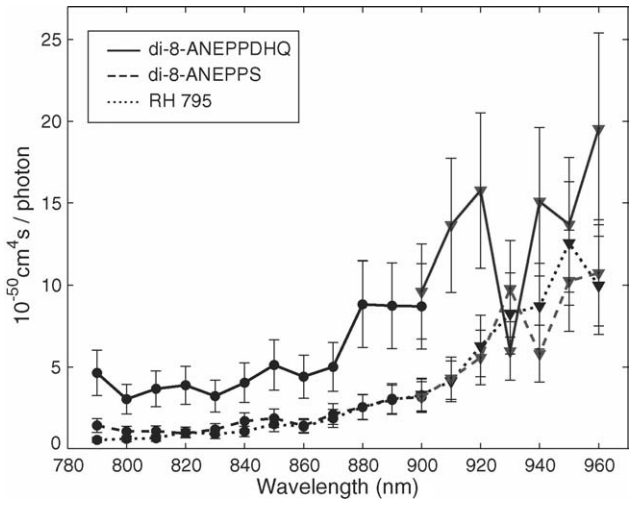

Fig. 5. Comparison of σ_2 for di-8-ANEPPDHQ, RH795, and di-8-ANEPPS. Solid line: di-8-ANEPPDHQ, dashed line: di-8-ANEPPS, dotted line: RH795, (●) mid-wavelength optics set (790–900 nm), (▼) long-wavelength optics set (900–960 nm).

4.3. Prospects for two-photon imaging using VSDs

Fluorescence-based scanning microscopy measures a relatively small number of photons per image pixel compared with reflectance or transmission bright-field video microscopy. Therefore to assess the practical utility of two-photon microscopy using voltage-sensitive dyes for measurement of membrane potential, we consider the case of shot-noise limited measurements. Fractional fluorescence ($\Delta F/F$) response following two-photon excitation of voltage-sensitive dyes varies considerably between dyes (Hess and Webb, 1998; Kuhn et al., 2004). While these studies have reported $\Delta F/F$ changes from 5% to 40% per 100 mV change in the membrane potential of cultured neurons in vitro, for the purpose of a conservative estimate of expected signal-to-noise ratio, we assume that with some expected non-specific dye-binding, the in vivo $\Delta F/F$ is ∼1% (as in one-photon fluorescence microscopy). To detect fractional fluorescence changes of 1% in a single measurement with a signal-to-noise ratio of greater than 1, it is necessary to detect $>10^4$ photons during the physiologically relevant sampling time. Using Eq. (5), we calculated the number of collected photons for a realistic epi-fluorescence microscope system (integration time = 100 μs, average power at objective focus = 10 mW, fluorescence collection efficiency = 10%, excitation wavelength = 930 nm, membrane-bound dye concentration = 10 μM, TPE cross-section = 16 GM, g_p = 0.588, laser repetition rate = 76 MHz, and laser pulse-width = 200 fs). Such a system would be capable of detecting 1% changes fluorescence with a signal-to-noise ratio of ∼2. This calculation suggests that the most suitable voltage-sensitive dyes for two-photon microscopy of neural network responses are di-8-ANEPPDHQ, di-8-ANEPPS, RH795, RH414 and RH421 at excitation wavelengths above 930 nm.

5. Conclusion

We have measured the TPE cross-sections in the range of 790–960 nm of seven commercially available voltage-sensitive dyes and two novel dyes obtained from other laboratories. Several of the fluorophores exhibited blueshifted spectral features. The novel naphthylstyryl pyridinium chimeric probe di-8-ANEPPDHQ was found to have large cross-sections compared with its constitutive structural elements, di-8-ANEPPS and RH795. Future work is underway to study the potentiometric properties of this set of voltage-sensitive dyes when excited via two-photon absorption.

Acknowledgements

The authors thank Eric P. Batchelor, Ana Lia Obaid, Kijoon Lee, Mark Goulian, and Mohammad Islam for technical assistance. We are also grateful to Winfried Denk, Samuel E. Hess, Stephen M. Potter, and Watt W. Webb for useful discussions. This work was supported by the David and Lucille Packard Foundation grant 2000-01737, by USPHS grants NS16824 and NS40966, and by NSF grants DMR-0203378 and DMR-079909.

References

Albota MA, Xu C, Webb WW. Two-photon excitation cross-sections of biomolecular probes from 690–960 nm. Appl Opt 1998;37:7352–6.

Angerer WE. SHG spectroscopy of gallium nitride thin films on sapphire with ultrashort pulses, Thesis. Philadelphia, PA: Department of Physics and Astronomy, University of Pennsylvania; 1998.

Angerer WE, Yang N, Yodh AG. Ultrafast second-harmonic generation spectroscopy of GaN thin films on sapphire. Phys Rev B 1999;59:2932–46.

Bedlack S R.S. Jr, Wei M, Loew LM. Localized membrane depolarizations and localized calcium influx during electric field-guided neurite growth. Neuron 1992;9:393–403.

Beeler TJ, Farmen RH, Martonosi AN. The mechanism of voltage-sensitive dye responses on sarcoplasmic reticulum. J Membr Biol 1981;62(1/2):113–37.

Birge RR. One-photon and two-photon excitation spectroscopy. In: Kliger D, editor. Ultrasensitive laser spectroscopy. New York: Academic Press; 1983.

Campagnola PJ, Wei M-D, Lewis A, Loew LM. High resolution nonlinear optical imaging of live cells by second harmonic generation. Biophys J 1999;77:3341–9.

Centonze VE, White JG. Multiphoton excitation provides optical sections from deeper within scattering specimens than confocal imaging. Biophys J 1998;75:2015–24.

Cohen LB, Salzberg BM, Davila HV, Ross WN, Landowne D, Waggoner AS, et al. Changes in axon fluorescence during activity: molecular probes of membrane potential. J Membr Biol 1974;19:1–36.

Cohen LB, Salzberg BM. Optical measurement of membrane potential. In: Reviews of physiology biochemistry and pharmacology. Berlin: Springer-Verlag; 1978.

Contreras D, Llinas R. Voltage-sensitive dye imaging of neocortical spatiotemporal dynamics to afferent activation frequency. J Neurosci 2001;21:9403–13.

Davila HV, Salzberg BM, Cohen LB, Waggoner AS. A large change in axon fluorescence that provides a promising method for measuring membrane potential. Nature (N Biol) 1973;241:159–60.

Denk W, Strickler JH, Webb WW. Two-photon laser scanning fluorescence microscopy. Science 1990;248:73–6.

Dombeck DA, Blanchard-Desce M, Webb WW. Optical recording of action potentials with second-harmonic generation microscopy. J Neurosci 2004;24:999–1003.

Fisher JAN, Civillico EF, Contreras D, Yodh AG. In-vivo fluorescence microscopy of neuronal activity in three dimensions by use of voltage-sensitive dyes. Opt Lett 2004;29:71–3.

Gogan P, Schmiedel-Jakob I, Chitti Y, Tyc-Dumont S. Fluorescence imaging of local membrane electric fields during the excitation of single neurons in culture. Biophys J 1995;69:299–310.

Grinvald A, Fine A, Farber IC, Hildesheim R. Fluorescence monitoring of electrical responses from small neurons and their processes. Biophys J 1983;42:195–8.

Grinvald A, Frostig RD, Lieke E, Hildesheim R. Optical imaging of neuronal activity. Physiol Rev 1988;68:1285–366.

Grinvald A, Lieke EE, Frostig RD, Hildesheim R. Cortical point-spread function and long-range lateral interactions revealed by real-time optical imaging of macaque monkey primary visual cortex. J Neurosci 1994;14:2545–68.

Hanna DC, Yuratich MA, Cotter D. Nonlinear optics of free atoms and molecules. New York: Springer-Verlag; 1979.

Hellwarth R, Christensen P. Nonlinear optical microscopic examination of structure in polycrystalline ZnSe. Opt Commun 1974;12:318–22.

Helmchen F, Fee MS, Tank DW, Denk W. A miniature head-mounted two-photon microscope: high-resolution brain imaging in freely moving animals. Neuron 2001;31:903–12.

Hess ST, Webb WW. Measurement of fluorescence signal of a voltage-sensitive dye using two-photon excitation. Biophys J 1998;74:201.

Hopt A, Neher E. Highly nonlinear photodamage in two-photon fluorescence microscopy. Biophys J 2001;80:2029–36.

Kleinfeld D, Delaney KR. Distributed representation of vibrissa movement in the upper layers of somatosensory cortex revealed with voltage sensitive dyes. J Comp Neurol 1996;375:89–108.

Kuhn B, Fromherz P, Denk W. High sensitivity of Stark-shift voltage-sensing dyes by one- or two-photon excitation near the red spectral edge. Biophys J 2004;87:631–9.

Lakowicz JR. Principles of fluorescence spectroscopy. New York: Klewer Academic Publishers/Plenum Press; 1999.

Llinas R. The intrinsic electrophysiological properties of mammalian neurons: insights into central nervous system function. Science 1988;242:1654–64.

Llinas R, Ribary U, Contreras D, Pedroarena C. The neuronal basis for consciousness. Phil Trans R Soc Lond B 1998;353:1841–9.

Orbach HS, Cohen LB. Optical monitoring of activity from many areas of the in vitro and in vivo salamander olfactory bulb: a new method for studying functional organization in the vertebrate central nervous system. J Neurosci 1983;3:2251–62.

Mainen ZF, Maletic-Savatic M, Shi SH, Hayashi Y, Malinow R, Svoboda K. Two-photon imaging in living brain slices. Methods 1999;18:231–9.

Mertz J, Moreaux L. Second-harmonic generation by focused excitation of inhomogeneously distributed scatterers. Opt Commun 2001;196:325–30.

Millard AC, Jin L, Lewis A, Loew LM. Direct measurement of the voltage sensitivity of second-harmonic generation from a membrane dye in patch-clamped cells. Opt Lett 2003;28:1221–3.

Obaid AL, Loew LM, Wuskell JP, Salzberg BM. Novel naphthylsturyl-pyridinium potentiometric dyes offer advantages for neural network analysis. J Neurosci Meth 2004;134:179–90.

Oheim M, Beaurepaire E, Chaigneau E, Mertz J, Charpak S. Two-photon microscopy in brain tissue: parameters influencing the imaging depth. J Neurosci Meth 2001;111:29–37.

Petersen CCH, Grinvald A, Sakmann B. Spatiotemporal dynamics of sensory responses in layer 2/3 of rat barrel cortex measured in-vivo by voltage-sensitive dye imaging combined with whole-cell voltage recordings and neuron reconstructions. J Neurosci 2003;23:1298–309.

Richards B, Wolf E. Electromagnetic diffraction in optical systems. II. Structure of the image field in an aplanatic system. Proc R Soc Lond Ser A 1959;253:358–79.

Salzberg BM. Optical recording of electrical activity in neurons using molecular probes. In: Barker J, McKelry J, editors. Current methods in cellular neurobiology. New York: John Wiley and Sons; 1983.

Salzberg BM, Davila HV, Cohen LB. Optical recording of impulses in individual neurons of an invertebrate central nervous system. Nature 1973;246:508–9.

Salzberg BM, Grinvald A, Cohen LB, Davila HV, Ross WN. Optical recording of neuronal activity in an invertebrate central nervous system: simultaneous monitoring of several neurons. J Neurophysiol 1977;40:1281–91.

Sheppards CJR, Matthews HJ. Imaging in high-aperture optical systems. J Opt Soc Am A 1987;4:1354–60.

Svoboda K, Helmchen F, Denk W, Tank DW. Spread of dendritic excitation in layer 2/3 pyramidal neurons in rat barrel cortex in-vivo. Nat Neurosci 1999;2:65–73.

Svoboda K, Denk W, Kleinfeld D, Tank DW. In-vivo dendritic calcium dynamics in neocortical pyramidal neurons. Nature 1997;385:161–5.

Stosiek C, Garaschuk O, Holthoff K, Konnerth A. In-vivo two-photon calcium imaging of neuronal networks. Proc Natl Acad Sci USA 2003;100:7319–24.

Sheppard CJR, Kompfner R, Gannaway J, Walsh D. Scanning harmonic optical microscope. IEEE J Quant Electron 1977;13E:100D.

Shoham D, Glaser DE, Arieli A, Kenet T, Wijnbergen C, Toledo Y, et al. Imaging cortical dynamics at high spatial and temporal resolution with novel blue voltage-sensitive dyes. Neuron 1999;24:791–802.

Sims PJ, Waggoner A, Wang C-H, Hoffman JF. Studies on the mechanism by which cyanine dyes measure membrane potential in red blood cells and phosphatidylcholine vesicles. Biochemistry 1974;13:3315–30.

Vergara J, Bezanilla F, Salzberg BM. Nile blue fluorescence signals from cut single muscle fibers under voltage or current clamp conditions. J Gen Physiol 1978;72:775–800.

Xu C. Two-photon cross-sections of indicators. In: Yuste R, Lanni F, Konnerth A, editors. Imaging neurons: a laboratory manual. Cold Spring Harbor, NY: Cold Spring Harbor Laboratory Press; 2000.

Xu C, Webb WW. Measurement of two-photon excitation cross-sections of molecular fluorophores with data from 690 to 1050 nM. J Opt Soc Am 1996;13:481–91.

Yoder E, Kleinfeld D. Cortical imaging through the intact mouse skull using two-photon excitation laser scanning microscopy. Microsc Res Tech 2002;56:304–5.

Yuste R, Tank DW, Kleinfeld D. Functional study of the rat cortical microcircuitry with voltage-sensitive dye imaging of neocortical slices. Cereb Cortex 1997;7:546–58.